Monthly Notices
of the
ROYAL ASTRONOMICAL SOCIETY

MNRAS **457,** 1224–1232 (2016) doi:10.1093/mnras/stw050

Radio detections of southern ultracool dwarfs

C. Lynch,[1,2★] T. Murphy,[1,2] V. Ravi,[3] G. Hobbs,[4] K. Lo[1,5] and C. Ward[1]

[1]*Sydney Institute for Astronomy, School of Physics, The University of Sydney, NSW 2006, Australia*
[2]*ARC Centre of Excellence for All-sky Astrophysics (CAASTRO)*
[3]*Cahill Centre for Astronomy and Astrophysics, MC 249-17, California Institute of Technology, Pasadena, CA 91125, USA*
[4]*Australia Telescope National Facility, CSIRO Astronomy and Space Science, PO Box 76, Epping, NSW 1710, Australia*
[5]*University College London Genetics Institute, University College London, London WC1E 6BT, UK*

Accepted 2016 January 6. Received 2016 January 5; in original form 2015 September 7

ABSTRACT

We report the results of a volume-limited survey using the Australia Telescope Compact Array to search for transient and quiescent radio emission from 15 Southern hemisphere ultracool dwarfs. We detect radio emission from 2MASSW J0004348−404405 increasing the number of radio loud ultracool dwarfs to 22. We also observe radio emission from 2MASS J10481463−3956062 and 2MASSI J0339352−352544, two sources with previous radio detections. The radio emission from the three detected sources shows no variability or flare emission. Modelling this quiescent emission we find that it is consistent with optically thin gyrosynchrotron emission from a magnetosphere with an emitting region radius of (1–2)R_*, magnetic field inclination 20°–80°, field strength ∼10–200 G, and power-law electron density $\sim 10^4$–10^8 cm^{-3}. Additionally, we place upper limits on four ultracool dwarfs with no previous radio observations. This increases the number of ultracool dwarfs studied at radio frequencies to 222. Analysing general trends of the radio emission for this sample of 15 sources, we find that the radio activity increases for later spectral types and more rapidly rotating objects. Furthermore, comparing the ratio of the radio to X-ray luminosities for these sources, we find 2MASS J10481463−3956062 and 2MASSI J0339352−352544 violate the Güdel–Benz relation by more than two orders of magnitude.

Key words: stars: activity – brown dwarfs – stars: low-mass – stars: magnetic field – radio continuum: stars.

1 INTRODUCTION

Surveys of chromospheric Hα and coronal X-ray emission from low-mass stars show a steady decline in magnetic activity strength beginning in late-type M dwarfs (e.g. Neuhäuser et al. 1999; Gizis et al. 2000; West et al. 2004; Williams, Cook & Berger 2014; Schmidt et al. 2015). The strength of activity in these two wavebands is frequently characterized by the ratio of the luminosity in the Hα/X-ray waveband to the bolometric luminosity (Hawley, Gizis & Reid 1996). The reduction in activity strength is thought to be associated with a decrease in plasma heating through the dissipation of magnetic fields (Mohanty et al. 2002). However, recent atmospheric modelling of late-type objects indicates that it is not unreasonable to expect observable Hα emission for these objects. The rarefied upper parts of the stellar atmospheres are found to be capable of magnetically coupling despite having a low levels of ionization (Rodríguez-Barrera et al. 2015). The decline in the magnetic activity strength traced by Hα and X-ray emission does not imply a drop in the fraction of active cool stars over later spectral types. The number of active systems, as indicated by Hα emission, is observed to increase across later spectral types and peaks between M9 and L0 objects (Schmidt et al. 2015). Additionally neither the magnetic field strength or filling factor for late-type objects is thought to decrease. In fact the detection of both quiescent and flaring non-thermal radio emission from some of the lowest mass stars and brown dwarfs (Berger et al. 2001; Berger 2002, 2006; Burgasser & Putman 2005; Osten & Jayawardhana 2006; Phan-Bao et al. 2007; Berger et al. 2009; McLean, Berger & Reiners 2012), collectively called ultracool dwarfs, confirms that at least some of these objects are still capable of generating strong magnetic fields.

Most radio loud ultracool dwarfs have a quiescent component, and in some cases, this component is found to vary with the rotation of the star (e.g. McLean et al. 2011). There is still some debate over the nature of the quiescent component where both depolarized electron cyclotron maser (ECM; Hallinan et al. 2007) and gyrosynchrotron emission from a non-thermal population of electrons (Berger 2002; Burgasser & Putman 2005; Osten et al. 2006a) are proposed sources for this emission. Furthermore, some radio loud ultracool dwarfs are observed to have strong radio flares that

★ E-mail: clynch@physics.usyd.edu.au

can be periodic. The ECM mechanism is generally accepted to be the source of the pulsed emission since it can account for the high brightness temperature, directivity, and circular polarization of this emission (Hallinan et al. 2006). These radio flares are sometimes associated with periodic variations in the optical band (Berger et al. 2009; Hallinan et al. 2015; Williams & Berger 2015). Recent simultaneous radio and optical observations of a late-type M dwarf showed that the observed modulation at both wavelengths could be accounted for by a propagating electron beam, powered by auroral currents, striking the stellar atmosphere (Hallinan et al. 2015). This results suggests that aurorae may be ubiquitous signatures of large-scale magnetospheres.

Radio surveys of ultracool dwarfs have found that about 9 per cent of these system are radio luminous, with 21 currently known radio loud ultracool dwarfs (Berger 2006; McLean et al. 2012; Antonova et al. 2013; Route & Wolszczan 2013; Kao et al. 2015). Correlations between the presence of transient or quiescent radio emission and other dwarf properties such as rotation and tracers of magnetic activity at other wavelengths (X-ray and Hα) are not well established. In fact, the radio luminosity of some detected systems is far in excess of the well-known Güdel–Benz (GB) relation (Güdel & Benz 1993), an empirically derived ratio between radio and X-ray luminosity that applies to magnetically active stars over a wide range of spectral types. The deviation from this relation observed in some ultracool dwarfs suggests that the chromospheric evaporation model usually applied to flare stars (Neupert 1968; Machado et al. 1980; Allred et al. 2006) may not apply to these objects. Furthermore, little is known about the geometry or strength of the magnetic fields in ultracool dwarfs as well as the mechanism that populates the magnetospheres with non-thermal electrons.

To address these issues, we carried out a volume-limited survey of a sample of 15 late-type M and L dwarfs located in the Southern hemisphere using the Australia Telescope Compact Array (ATCA). The Compact Array Broad-band Backend (Wilson et al. 2011) allows for a bandwidth of 2 GHz per polarization in each of two independently tuneable intermediate frequency (IF) bands. These wideband capabilities of ATCA easily provide detailed information about how observed radio pulses and quiescent emission vary in time and frequency. Such a characterization is required if we want to constrain the magnetospheric parameters and geometry of ultracool dwarfs (Section 4). Additionally, to understand general trends of radio emission from ultracool dwarfs with regards to their other physical properties, our observations are augmented with values for projected rotational velocities ($v\sin(i)$), Hα and X-ray luminosities from the literature (Section 5).

2 OBSERVATIONS AND DATA REDUCTION

The sample of 15 ultracool dwarfs were selected form the all-sky-volume-limited compilations of late-M (Reiners & Basri 2009) and L (Reid et al. 2008) dwarfs. From these two catalogues we selected sources with distances <10 pc and located in the Southern hemisphere. This selection of sources consists of eight M dwarfs and seven L dwarfs, with spectral types ranging from M7.0 to L8.0. Additionally, this selection of sources includes three known radio loud ultracool dwarfs: 2MASS J1456−2809 (Burgasser & Putman 2005; Osten & Wolk 2009), 2MASS J10481463−3956062 (Burgasser & Putman 2005; Ravi et al. 2011), and 2MASSI J0339352−352544 (Berger et al. 2001). Further details about the selected survey targets are given in Table 1.

The observations of the 15 ultracool dwarfs were carried out with ATCA in its fully extended 6 km configurations during the time period between 2010 April and June. During our observations the two IF bands were centred on 5.5 and 9.0 GHz simultaneously. A log of these observations is given in Table 2.

The visibility data were reduced using the standard routines in the MIRIAD environment (Sault, Teuben & Wright 1995). The flux scale and bandpass response were determined from the ATCA primary calibrators, either PKS B1934-638 or PKS B0823-500. Observations of a bright, compact secondary calibrator was used to calibrate the complex gains and leakage between the orthogonal linear feeds in each antenna. Observations of the secondary calibrators (listed in Table 2) were carried out every 20 min, for 1.3 min. The flare emission observed from some ultracool dwarfs can be confused with low level radio frequency interference (RFI) peaks. However, the flares from ultracool dwarfs are not strongly linearly polarized. So to avoid confusing RFI with a source flare, we first identified and flagged RFI in the Stokes Q and U polarizations and then

Table 1. Properties of the survey sources.

2MASS Number	RA	Dec.	Spectral type	Distance (pc)	$v\sin(i)$ (km s^{-1})	$L_{\rm bol}$ ($L_\odot$)	$L_x/L_{\rm bol}$	$L_{\rm H\alpha}/L_{\rm bol}$	Reference[a]
10481258–1120082	10 48 12.8	−11 20 18.9	M7.0	4.5	3.0	−3.16	−4.43	−4.63	1,6
14563831–2809473	14 56 38.1	−28 09 53.3	M7.0	7.0	8.0	−3.29	−4.00	−4.02	1, 5, 7
11554286–2224586	11 55 42.7	−22 24 59.6	M7.5	9.7	33.0	−3.30	−4.40	−4.58	1, 6, 12
10481463–3956062	10 48 13.5	−39 56 17.0	M8.0	4.0	18.0	−3.39	−5.00	−5.15	1, 5, 8
00244419–2708242	00 24 44.1	−27 08 19.7	M8.5	7.71	9.0	−3.25	–	−4.62	11
0339352–352544	03 39 35.5	−35 25 40.8	M9.0	5.0	26.0	−3.79	−3.70	−5.30	1, 2
03341218–4953322	03 34 13.3	−49 53 28.6	M9.0	8.20	–	–	–	<5.32	11
0853362–032932	08 53 35.9	−03 29 33.5	M9.0	9.0	13.5	−3.49	−3.70	−3.93	3
1507476–162738	15 07 47.6	−16 27 44.9	L5.0	7.3	32.0	−4.23	<-4.50	−8.18	1, 4
08354256–0819237	08 35 42.3	−08 19 21.7	L5.0	9.0	23.0	−4.60	–	−7.42	1, 4, 5
0004348-404405	00 04 35.4	−40 44 21.8	L5.0	10.0	42.0	−4.67	–	− 7.42	1
17502484–0016151	17 50 24.6	+00 16 13.7	L5.5	8.0	–	–	–	–	1
0340094–672405	03 40 09.3	−67 24 08.7	L8.0	9.90	–	–	–	–	10
02550357–4700509	02 55 04.0	−47 00 54.9	L8.0	4.97	67	−4.80	<−4.70	<−8.28	9, 12
02572581–3105523	02 57 26.1	−31 05 50.0	L8.0	9.6 0	–	−4.82	–	–	1

[a]References: (1) Antonova et al. (2013); (2) Berger et al. (2001); (3) Berger (2002); (4) Berger (2006); (5) Burgasser & Putman (2005); (6) McLean et al. (2012); (7)Osten & Wolk (2009); (8) Ravi et al. (2011); (9) Reid et al. (2008); (10) Reiners & Basri (2008); (11) Reiners & Basri (2010); (12) Williams et al. (2014).

Table 2. Log of observations.

2MASS number	Observation date	ATCA configuration[a]	Primary calibrator	Secondary calibrator
10481258–1120082	17 Apr 2010 06:41 – 17 Apr 2010 16:39	6A	PKS B0823-500	1045−188
14563831–2809473	12 Apr 2010 09:32 – 12 Apr 2010 21:59	6A	PKS B1934-638	1519−273
11554286–2224586	19 Apr 2010 05:49 – 19 Apr 2010 16:22	6A	PKS B0823-500	1143−245
10481463–3956062	18 Apr 2010 05:12 – 18 Apr 2010 15:43	6A	PKS B0823-500	1104−445
00244419–2708242	24 Apr 2010 18:18 – 25 Apr 2010 06:11	6A	PKS B1934-638	2357−318
0339352–352544	30 May 2010 18:55 – 31 May 2010 07:08	6C	PKS B1934-638	0405−331
03341218–4953322	29 May 2010 18:43 – 30 May 2010 06:30	6C	PKS B1934-638	0302−623
0853362–032932	30 Apr 2010 04:12 – 30 Apr 2010 13:36	6C	PKS B1934-638	0906+015
1507476–162738	14 Apr 2010 10:13 – 14 Apr 2010 21:05	6A	PKS B1934-638	1504−166
08354256–0819237	21 Apr 2010 03:16 – 21 Apr 2010 14:01	6A	PKS B1934-638	0859−140
0004348–404405	25 Apr 2010 17:47 – 26 Apr 2010 05:31	6A	PKS B1934-638	0022−423
217502484–0016151	13 Apr 2010 13:35 – 13 Apr 2010 22:44	6A	PKS B1934-638	1741−038
0340094–672405	22 Apr 2010 22:03 – 23 Apr 2010 10:00	6A	PKS B1934-638	0252−712
02550357–4700509	27 Apr 2010 17:17 – 28 Apr 2010 05:20	6C	PKS B0823-500	0252−549
02572581–3105523	28 May 2010 18:11 – 29 May 2010 06:02	6C	PKS B1934-638	0237−233

[a]The labels refer to different variants of the antenna spacings; these are defined at: http://www.narrabri.atnf.csiro.au/operations/array_configurations/configurations.html.

Table 3. Characteristics of the radio emission.

2MASS number	$S_{5.5\,\mathrm{GHz}}(I)^a$ (μJy)	$S_{5.5\,\mathrm{GHz}}(V)^a$ (μJy)	$S_{9.0\mathrm{GHz}}(I)^a$ (μJy)	$S_{9.0\mathrm{GHz}}(V)^a$ (μJy)	$\alpha_{4.7\text{–}9.7\,\mathrm{GHz}}$	T_B (K)
10481258–1120082	<44.7	<26.7	<34.5	<31.8	–	$<5.98\times10^7$
14563831–2809473	<29.9	<29.0	<37.4	<36.8	–	$<9.69\times10^7$
11554286–2224586	<31.2	<25.8	<34.8	<34.2	–	$<1.94\times10^8$
10481463–3956062	211.9±8.2	<29.1	131.4±10.8	<31.8	−1.1± 0.11	2.23×10^8
00244419–2708242	<111.0	<37.8	<237.0	<48.9	–	$<4.36\times10^8$
0339352–352544	137.6±10.5	73.0±10.0	90.7±17.6	<57.3	−0.97± 0.32	2.26×10^8
03341218–4953322	<29.4	<26.1	<37.8	<42.0	–	$<1.31\times10^8$
0853362–032932	<42.9	<35.4	<53.7	<50.4	–	$<2.30\times10^8$
1507476–162738	<37.6	<28.5	<36.6	<35.4	–	$<3.58\times10^8$
08354256–0819237	<32.0	<28.0	<42.0	<41.0	–	$<1.71\times10^8$
0004348–404405	100.0±8.3	44.3±8.2	<39.9	<38.4	<−0.74	6.61×10^8
17502484–0016151	<81	<36	<51	<39	–	$<3.43\times10^8$
0340094–672405	<27.0	<27.3	<39.0	<39.0	–	$<1.75\times10^8$
02550357–4700509	<30.9	<26.7	<34.6	<31.8	–	$<5.05\times10^7$
02572581–3105523	<66.0	<35.4	<63.0	<60.0	–	$<4.02\times10^8$

[a]Upper limits listed are 3σ limits based on the RMS values measured in the images for each source.

extend these flags to the other polarizations. To carry out this flagging scheme we used the MIRIAD flagging tools PGFLAG and BLFLAG.

After calibration, the visibility data for each source was inverted and cleaned using the MIRIAD tasks INVERT, CLEAN, and RESTOR. Bright sources located in the same field as the target source were identified and removed. This process involved using the CLEAN components for each of the bright sources, while masking the location of the target ultracool dwarf, and subtracting the source from the visibility data using the MIRIAD task UVMODEL. The phase centre of the resulting visibility data was shifted to the location of the target ultracool dwarf using the MIRIAD task UVEDIT and then inverted and cleaned in the standard fashion.

To search for radio emission from each of the sources, we made images for both the 5.5 and 9.0 GHz frequency bands where we averaged over the full ∼12 h of observation and 2 GHz bandwidth, to ensure the best signal-to-noise ratio. We fit these images using the Common Astronomy Software Application (CASA; McMullin et al. 2007) tool IMSTAT, which reports the statistics for a supplied region of an image. To determine if a source has detectable radio emission, we compared the measured peak flux density at the location of the source to the image RMS determined from a fit to a region centred on the source position with dimensions were six times the size of the restoring beam. We considered peak flux densities greater than three times the image RMS as detections. These fits were carried out in both the Stokes I and V images and the results are listed in Table 3.

For sources observed with detectable radio emission in either of these two 2 GHz images, additional I and V images using 512 MHz frequency averaging were made to constrain the spectral index and polarization frequency dependence. These 512 MHz images were then fit using the same method detailed above. By vector averaging the real components of the visibilities in time bins of 10, 30, and 60 s over the two 2.0 GHz frequency bins, light curves were created to search for variability (Section 3.1).

3 DETECTIONS

From fits to the 2 GHz frequency averaged images, we find only three of our 15 target ultracool dwarfs have detectable levels of Stokes I emission in at least one of the two observing frequency bands, 2MASS J10481463−3956062 (hereafter 2MASS J1048−3956), 2MASSI J0339352−352544

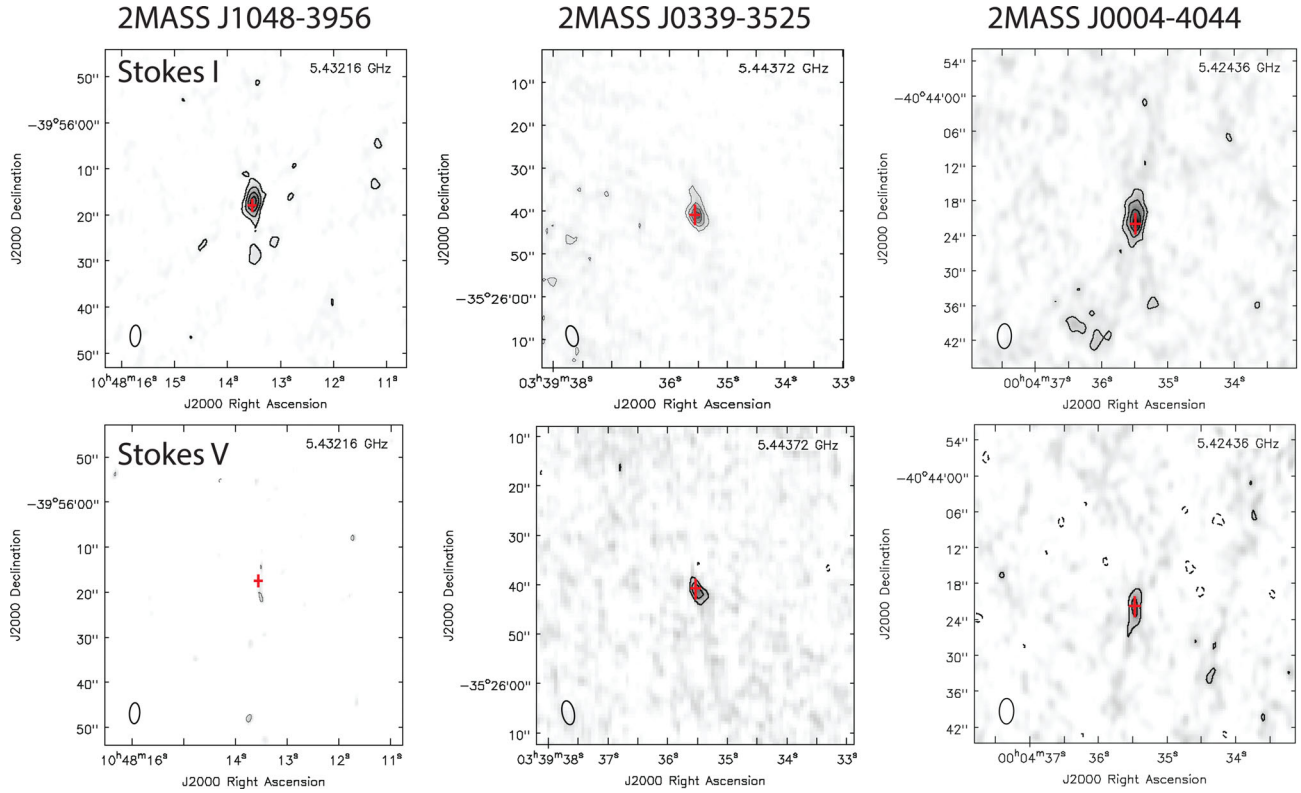

Figure 1. Radio images for 2MASS J1048−3956 (left-hand column), 2MASS J0339−3525 (middle column), and 2MASS J0004−4044 (right-hand column) in Stokes I (top-row) and Stokes V (bottom-row) at 5.5 GHz. Additionally, contours are overlaid with levels at 3, 9, 18, 27 times the Stokes I RMS value of 8.2 μJy for 2MASS J1048−3956 and 3, 6, 9, 12 20 times the Stokes I RMS values of 10.5 and 8.3 μJy for 2MASS J0339−3525 and 2MASS J0004−4044, respectively. For all sources the Stokes V contours are −10, −5, −3, 3, 5, 10 times the RMS values of 9.7 μJy for 2MASS J1048−3956, 17.6 μJy for 2MASS J0339−3525, and 13.3 μJy for 2MASS J0004−4044.

(hereafter 2MASS J0339−3525), and 2MASSW J0004348−404405 (hereafter 2MASS J0004−4044). The Stokes I and V images for these three sources at 5.5 GHz and 9.0 GHz are shown in Figs 1 and 2, respectively. The flux density peaks in each of these images lie within the mean beam size of the predicted positions determined from the 2MASS astrometry (Cutri et al. 2003) and proper motion measurements from the literature (Deacon, Hambly & Cooke 2005; Schmidt et al. 2007; Faherty et al. 2009).

Both 2MASS J1048−3956 and 2MASS J0339−3525 have previous radio detections, while the detection of 2MASS J0004−4044 is the first. Additionally, this survey includes radio limits on four sources, 2MASSI J0340094−672405, 2MASS J02550357−4700509, 2MASS J03341218−4953322, and 2MASS J00244419−2708242, with no previous radio observations. Combining our results with that of Antonova et al. (2013), Route & Wolszczan (2013), Burgasser et al. (2013, 2015), and Kao et al. (2015), the number of ultracool dwarfs studied at radio frequencies is now 222, with 22 sources observed to have radio emission. From these numbers, ∼10 per cent of ultracool dwarfs are observed to have radio emission. This is higher than the estimate by Antonova et al. (2013) who get ∼6 per cent when they consider only their observations and that of McLean et al. (2012). Additionally using this set of observations, Antonova et al. (2013) note that the majority of the ultracool dwarfs with observed radio emission have a spectral type between M7 and L3.5. However, this result may be due to the small number of observations of objects with spectral types >L3.5 included in their sample. If we add to the Antonova et al. (2013) sample the results of Burgasser et al. (2013), Route & Wolszczan (2013), Kao et al. (2015), and our own radio detections, the fraction of ultracool dwarfs with observable radio emission remains constant (∼10 per cent) across the spectral type range M7–T8.

3.1 Variability

To search for burst emission and any potential periodicity in the detected sources, we constructed light curves of the real visibilities in Stokes I and V for 2MASS J1048−3956, 2MASS J0339−3525, and 2MASS J0004−4044. These light curves were made for 1, 0.5, and 0.1 min time averaged bins and 512 MHz, 1 GHz, and 2 GHz frequency averaged bins. In all combinations of averaging we do not detect any burst emission or variability in the quiescent component.

We carried out a Lomb–Scargle analysis (Lomb 1976; Scargle 1982) using the astroML scientific python modules (VanderPlas et al. 2012) to test the significance of the non-variability. The periodograms of the three sources with observed radio emission are shown in Fig. 3. The dashed lines indicate false alarm probabilities for the 99, 90, and 61 per cent levels. For all three source there are no significant peaks in the Lomb–Scargle power spectrum for variability on time-scales less than an hour up to 12 h.

4 CHARACTERISING THE QUIESCENT EMISSION

2MASS J1048−3956, 2MASS J0339−3525, and 2MASS J0004−4044 all have detectable levels of Stokes I emission at

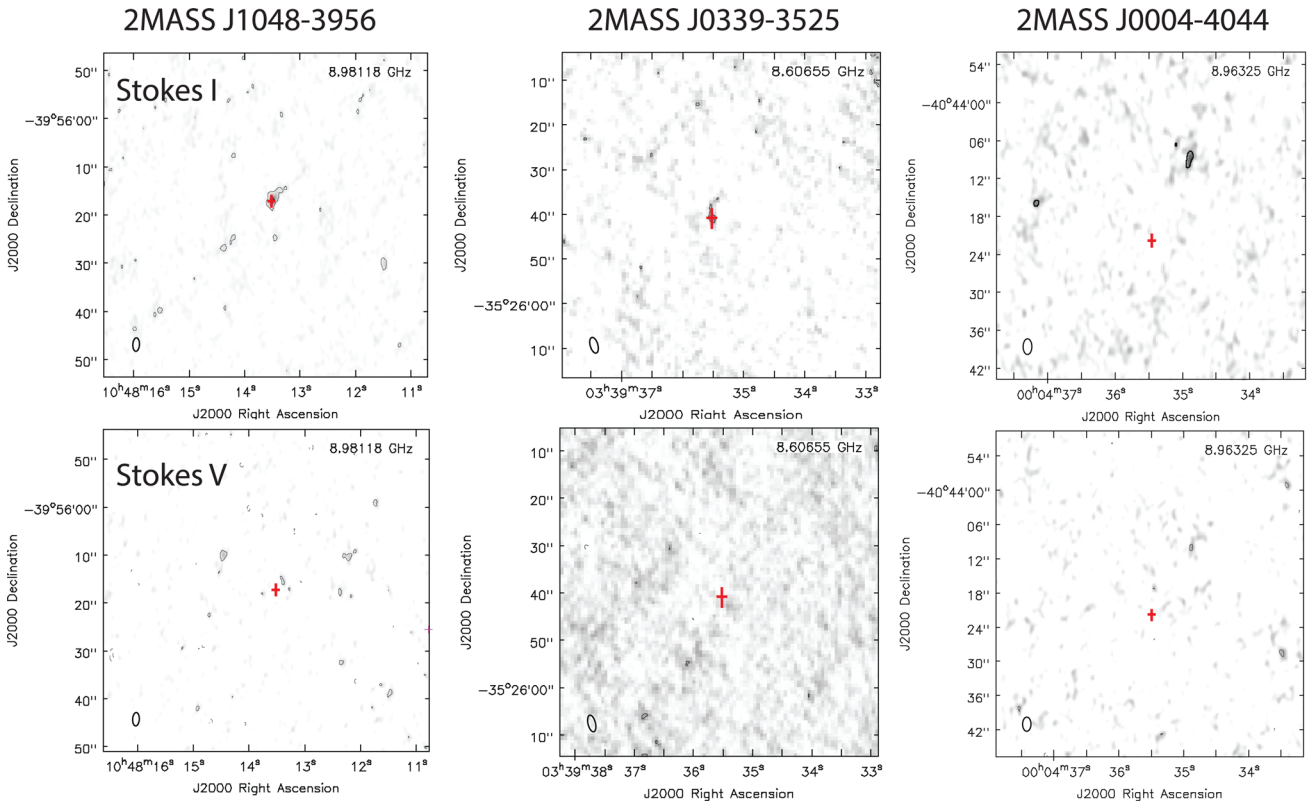

Figure 2. Radio image for 2MASS J1048−3956 (left-hand column), 2MASS J0339−3525 (middle column), and 2MASS J0004−4044 (right-hand column) in Stokes I (top-row) and Stokes V (bottom-row) at 9.0 GHz. Additionally, contours are overlaid with levels at 3, 9, 18, 27 times the Stokes I RMS value of 10.6 μJy for 2MASS J1048−3956 and 3, 6, 9, 12 20 times the Stokes I RMS values of 10.0 and 8.2 μJy for 2MASS J0339−3525 and 2MASS J0004−4044, respectively. For all sources the Stokes V contours are −10, −5, −3, 3, 5, 10 times the RMS values of 10.6 μJy for 2MASS J1048−3956, 19.1 μJy for 2MASS J0339−3525, and 12.8 μJy for 2MASS J0004−4044.

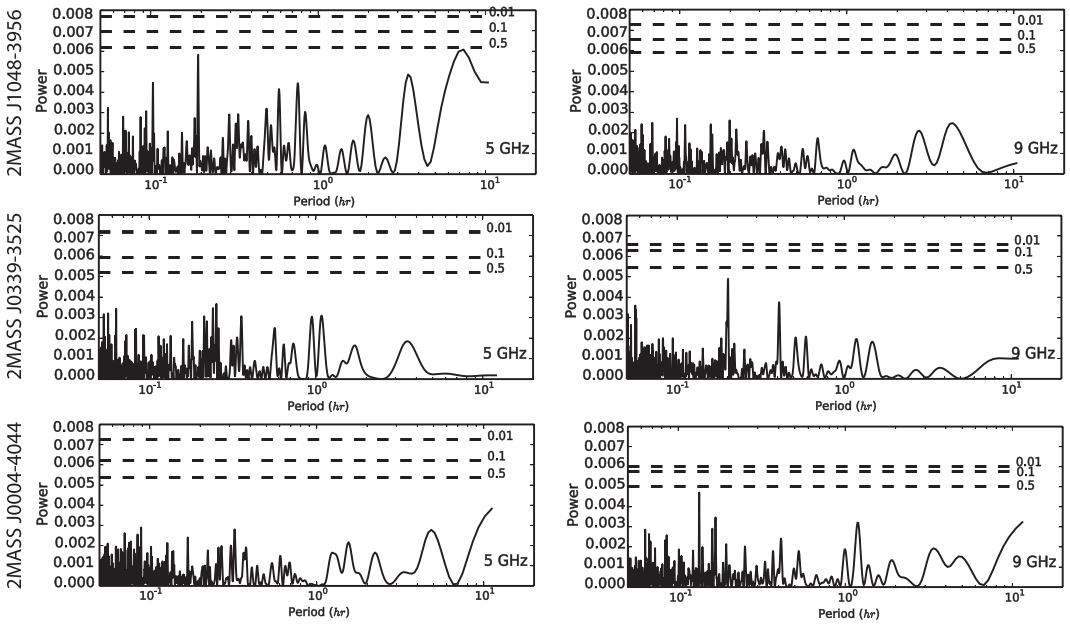

Figure 3. Lomb–Scargle periodogram of the 10 s time averaged and 2 GHz frequency averaged, Stokes I flux values for 2MASS J1048−3956 (top), 2MASS J0339−3525 (middle), and 2MASS J0004−4044 (bottom). The periodograms are calculated for both the 5 GHz (left-hand column) and 9 GHz (right-hand column) frequency bands. Dashed lines indicate false alarm probabilities of 0.01 (99 per cent), 0.1 (90 per cent), and 0.5 (61 per cent). We did not detect significant variability in these three sources.

5.5 GHz. For both 2MASS J0339−3525 and 2MASS J0004−4044 the 5.5 GHz emission is also observed to be polarized, with polarization fractions of 0.53 for 2MASS J0339−3525 and 0.44 for 2MASS J0004−4044. At 9 GHz the radio emission from 2MASS J0004−4044 is undetectable, however, for both 2MASS J0339−3525 and 2MASS J1048−3956 we still detect Stokes I emission from these sources. We do not detect any Stokes V emission for any of the sources at this higher frequency.

4.1 Spectral indices

We did a least-squares fit to the measured Stokes I values from the 512 MHz images to constrain spectral indices for the three detected sources (see Table 3) between 4.7 and 9.7 GHz. For all three sources the emission drops steeply with increasing frequency and shows no signs of a turn-over in the lower observing frequency band.

Comparing the spectral indices we calculate for 2MASS J0339−3525 and 2MASS J1048−3956 to previously cited values, we find that they do not agree. For 2MASS J0339−3525, Berger et al. (2001) constrain the spectral index to be 2.1±0.3 between 4 and 8 GHz, indicating optically thick emission. The discrepancy between our result and that of Berger et al. (2001) is most likely because Berger et al. (2001) include both flare and quiescent emission in their analysis while we only consider the quiescent component. Yet note that the measured flux densities from Berger et al. (2001) vary by more than a factor of 2 over the 3 months covered by their observations. This flux density variation could also be related to a variation in the spectral index. The quiescent radio emission from 2MASS J1048−3956 has been studied over a wide range of radio frequencies (∼4.0–20 GHz) by Ravi et al. (2011) who fit a spectral index of $\alpha = 1.71 \pm 0.09$ to the observed radio emission. The smaller frequency coverage of our observations could be the cause of this difference. However, similar to 2MASS J0339−3525, the 4–9 GHz emission of 2MASS J1048−3956 is variable on long-time-scales where the radio emission previously observed by Ravi et al. (2011) has a slightly higher flux density and is circularly polarized with a polarization fraction of 0.25–0.4. Long-term variability in the measured flux densities and polarization of UCDs has been observed in several other cases (McLean et al. 2012) and may indicate a significant change in the physical characteristics of the emitting regions in these sources. Such variability is also well known in the case of radio flares from close stellar binaries and are attributed to changes in energisation (e.g. RS CVns; Mutel et al. 1998; Richards et al. 2003).

4.2 Brightness temperatures

In order to assess the origin of the radio emission, we can calculate the brightness temperature of the observed emission. For a radio source at a distance d with an emitting volume of radius R, and flux density S_ν at frequency ν, the brightness temperature is given by

$$T_b = 2.5 \times 10^9 \left(\frac{S_\nu}{\mathrm{mJy}}\right) \left(\frac{\nu}{\mathrm{GHz}}\right)^{-2} \left(\frac{d}{\mathrm{pc}}\right)^2 \left(\frac{R}{R_\mathrm{J}}\right)^{-2} \mathrm{K}, \quad (1)$$

where R_J is the radius of Jupiter and is the typical radius of very low mass stars and brown dwarfs (Burrows et al. 2001). Assuming M-type stellar coronal dimensions of (1–2)R_* (Leto et al. 2000), the measured flux densities and appropriate upper limits for the non-detections imply brightness temperatures in the range of (0.5–6)× 10^8 K at 5.5 GHz (see Table 3).

Table 4. Model parameters.

2MASS number	R (R_*)	θ_B	B (G)	log (N_e) (cm^{-3})
10481463–3956062	1.0–2.0	40°–80°	10–70	6.0–8.0
0339352–352544	1.0–2.0	20°–60°	20–223	4.1–6.8
0004348–404405	1.5–2.0	40°–60°	73–231	4.5–6.2

4.3 Origins for the emission

The high brightness temperatures, combined with the spectral indices, and the measured circular polarization of 2MASS J0339−3525 and 2MASS J0004−4044, rule out thermal bremsstrahlung emission and we find the emission to be more consistent with gyrosynchrotron emission from a non-thermal population of accelerated electrons (Dulk 1985). To model the observed emission characteristics, we used the expressions found in Robinson & Melrose (1984) for the absorption and emission coefficients of gyrosynchrotron emission from mildly relativistic electrons with a power-law electron distribution given by

$$N_e(E) = K E^{-\delta},$$

where $K = N_0(\delta - 1){E_0}^{\delta - 1}$ and is δ the energy index, and with a low-energy cutoff $E_0 = 10$ keV.

Such a model requires some knowledge of the magnetic geometry for the ultracool dwarf, specifically the angle of inclination between the line of sight and the magnetic axis, θ_B. An estimate of this inclination angle can be obtained from observed variability in optical emission. However, 2MASS J1048−3956, 2MASS J0339−3526, and 2MASS J0004−4044 are observed to have little variability at these wavelengths (Schmidt et al. 2007; Guenther et al. 2009; Stelzer et al. 2012; Crossfield 2014). Thus, to characterize the plasma conditions responsible for this emission, we construct a simple coronal model consisting of a homogenous population of mildly relativistic power-law electrons spiralling in a uniform magnetic field. This simple model allows us to make an order-of-magnitude estimate for the power-law electron density and magnetic field strength without making assumptions concerning the geometry of the magnetic field.

For this model we assumed the radius of the emitting region to range from (1–2)R_*, consistent with estimates for the emitting region dimension on M dwarfs (Leto et al. 2000), and varied the emitting volume, the strength and orientation of the magnetic field, and the non-thermal electron density to best fit the measured spectral energy distribution (SED) and fractional circular polarization for each source. Since the SED for 2MASS J1048−3956, 2MASS J0339−3525, and 2MASS J0004−4044 is consistent with optically thin gyrosynchrotron emission, we constrain the energy index δ for the model using the approximation (Dulk 1985)

$$\delta = (1.22 - \alpha_{4.7\text{-}9.7\,\mathrm{GHz}})/0.9$$

and the spectral indices given in Table 3. Additionally, the optically thin assumption implies that the gyrosynchrotron turn-over frequency is less than 4.7 GHz and further limits the range of suitable model parameters.

The model parameters that reproduce the observed Stokes I and V emission for 2MASS J1048−3956, 2MASS J0339−3525, and 2MASS J0004−4044 are listed in Table 4. Generally the range of values for the densities, magnetic field orientations and strengths, and the emission volumes are consistent with previous constraints found for ultracool dwarf magnetospheres (Burgasser & Putman 2005; Osten et al. 2006b; Ravi et al. 2011; Lynch, Mutel & Güdel 2015). Sample SED's are shown in Fig. 4, along with the

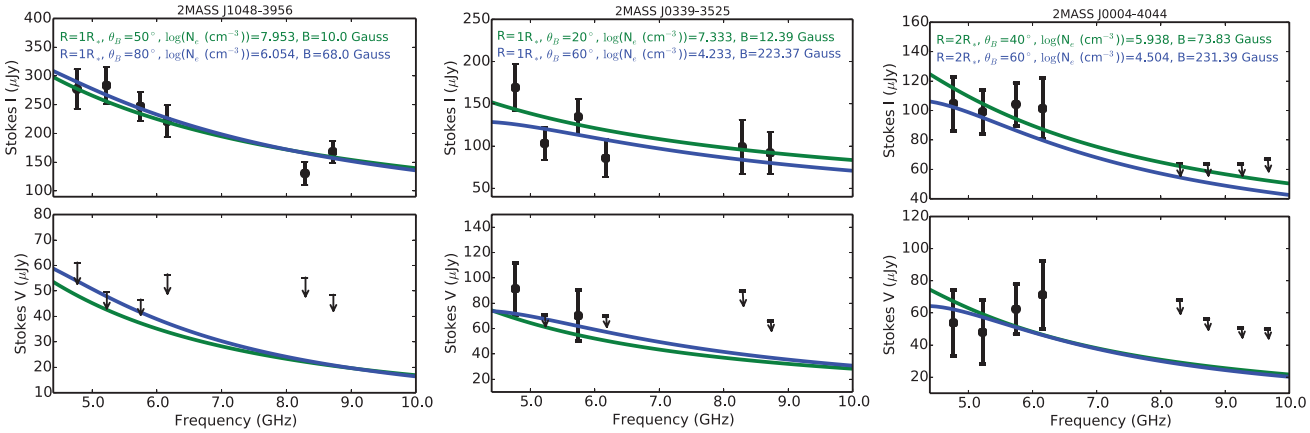

Figure 4. Comparisons between two representative model curves and the measured Stokes I (top) and Stokes V (bottom) flux densities for 2MASS J1048−3956 (left), 2MASS J0339−3525 (middle), and 2MASS J0004−4044 (right). The measured values result from fits to the 512 MHz images for each source. The two different colours represent two different sets of model parameters that fall within the values listed in table 4.

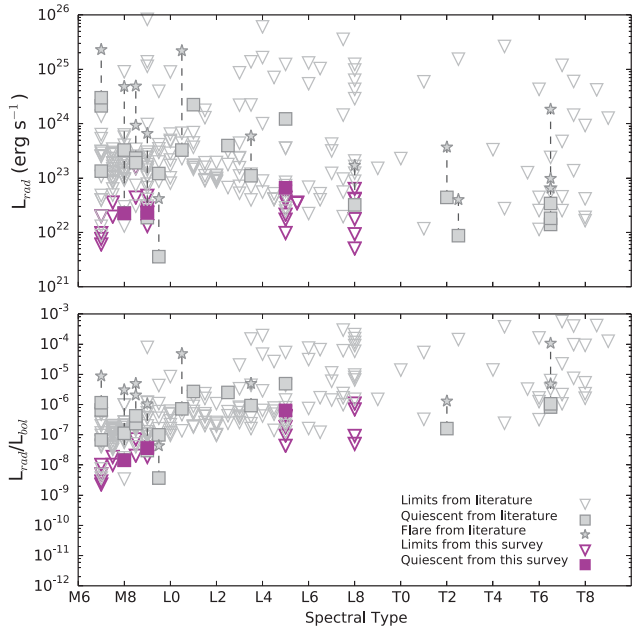

Figure 5. (Top) Radio luminosity and (bottom) ratio of the radio to bolometric luminosity as a function of spectral type for ultracool dwarfs. Shown are flares (stars), quiescent emission (squares), and upper limits (open triangles). The results from this survey are magenta and values from the literature (Antonova et al. 2013; Burgasser et al. 2013, 2015; Route & Wolszczan 2013; Kao et al. 2015) are grey. For objects with observed quiescent and flare emission, the values are connected by dashed lines.

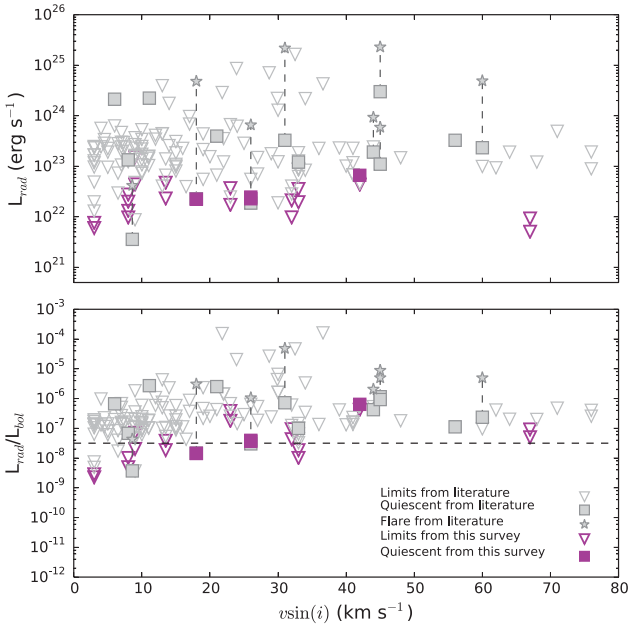

Figure 6. (Top) Radio luminosity and (bottom) ratio of the radio to bolometric luminosity as a function of projected rotational velocity for ultracool dwarfs. Upper limits (open triangles), flares (stars), and quiescent emission (squares) are shown for both this survey (magenta) and the literature (grey; Antonova et al. 2013; Burgasser et al. 2013, 2015; Route & Wolszczan 2013). The dashed line in the bottom panel indicates the radio activity-rotation saturation level for early type M dwarfs from McLean et al. (2012).

corresponding observed fluxes in the 512 MHz images. The model parameters for each curve are annotated in the figure, where the colour of the text corresponds to the colour of the appropriate model curve. The SED fits are quite acceptable, with most of the model fluxes agreeing with upper limits and measured flux densities for both the Stokes I and V emission.

5 RADIO EMISSION TRENDS

To put the results of our survey into context, we compare our radio results with that of previous radio surveys in Figs 5 and 6. In these figures our measurements are the magenta points and the grey points are from Route & Wolszczan (2013), Antonova et al. (2013), Burgasser et al. (2013, 2015), and Kao et al. (2015), where appropriate. In these figures we include upper limits (open triangles), quiescent emission (squares), and flares (stars). We find that our upper limits on the radio luminosity are lower than those placed by the previous surveys but are still comparable to the detected quiescent emission from the least bright sources. The observed luminosities for 2MASS J1048−3956 and 2MASS J0339−3525 are consistent with those from previous surveys.

As a function of spectral type (Fig. 5), we observe the radio luminosity to be constant, agreeing with previous radio surveys which found $L_{\rm rad} \sim 10^{23\pm0.5}$ erg s^{-1} for objects with spectral type M0–L5 (Berger et al. 2010). Furthermore, when we compare the ratio of radio to bolometric luminosity to spectral type, we observe

the previously noted trend of increased activity with later spectral type. This is in contrast with observations of other activity tracers, such as Hα and X-ray emission, where this ratio decreases past spectral type M7 (Berger et al. 2010).

Fig. 6 shows the radio luminosity and ratio of radio to bolometric luminosity as a function of rotation rate. 2MASS J1048−3956, 2MASS J0339−3525, and 2MASS J0004−4044 are all rapid rotators with $v\sin(i) \gtrsim 20$ km s^{-1}. The radio luminosities for these three sources are observed to be fairly constant with rotation rate agreeing with the previous results of McLean et al. (2012). However, note that rapid rotation does not necessarily indicate a source will have observable radio emission. In fact the most rapidly rotating source in our sample of 15, 2MASS J02550357−4700509, has an upper limit of $L_{\rm rad} \sim 9 \times 10^{11}$ erg s^{-1}, which is lower than the luminosity of the detected sources.

If we look at the ratio of the radio to bolometric luminosity for this sample of sources we see that 2MASS J1048−3956 and 2MASS J0339−3525 have ratios that lie along the radio activity-rotation saturation level observed in early-M dwarfs, $L_{\rm rad}/L_{\rm bol} \sim 10^{-7.5}$ (McLean et al. 2012). However, note that sources with rotation rates $\gtrsim$30 km s^{-1}, including our observation of 2MASS J0004−4044, all lie above the early-M dwarf saturation level. As noted by McLean et al. (2012) these more rapidly rotating sources appear to tend towards the higher ratio of radio to bolometric luminosity of $L_{\rm rad}/L_{\rm bol} \sim 10^{-6.5}$.

5.1 X-ray/Radio correlation

As mentioned in Section 1, there is a tight correlation between the radio and X-ray emission for coronally active stars ranging from spectral type F to mid-M, where $L_\nu/L_x \sim 10^{-15.5}$ Hz^{-1} (Güdel & Benz 1993; Benz & Guedel 1994). The first radio observation of an ultracool dwarf found $L_\nu/L_x \sim 10^{-11.5}$ Hz^{-1} for this source (Berger et al. 2001), suggesting that the GB relation may be severely violated by these objects. Subsequent radio detections of ultracool dwarfs have found that these objects display a wide range of behaviour with regard to the GB relation, where some sources are strongly radio overluminous varying from the GB relation by several orders of magnitude, while others could be consistent with this relation (Williams et al. 2014).

Using the radio luminosities, L_ν, for our 15 sources as well as X-ray luminosities, L_x, from the literature, we can determine if these sources fall along the GB relation. Fig. 7 shows this comparison, where we have also plotted the observed data from Güdel & Benz (1993, grey points) and the linear fit of $\log(L_\nu) = 1.36[\log(L_x) - 18.9]$ to this data (Berger et al. 2010). The scatter of the data from Güdel & Benz (1993) around this line is 0.6 dex when we measure the deviation at a fixed L_x. The relative scatter of the data to the best-fitting line (i.e. measured perpendicular to the line) is 0.2 dex. In order to be consistent with the analysis of Williams et al. (2014), we define the difference between the measured ratio of radio to X-ray luminosity and the GB relation as the perpendicular distance between the measured value and the best-fitting line.

Out of the three sources in our survey with detectable levels of radio emission only 2MASS J1048−3956 and 2MASS J0339−3525 have measured X-ray luminosities in the literature. Comparing the ratio of the radio to X-ray luminosity for these two sources we find that they differ from the GB relation by 2.5 dex and 1.7 dex, for 2MASS J1048−3956 and 2MASS J0339−3525, respectively. The variation from the GB relation for these two sources, while significant, is not nearly as extreme as the variation observed for other ultracool dwarfs (e.g. TVLM-513; Berger et al. 2008; Williams et al. 2014).

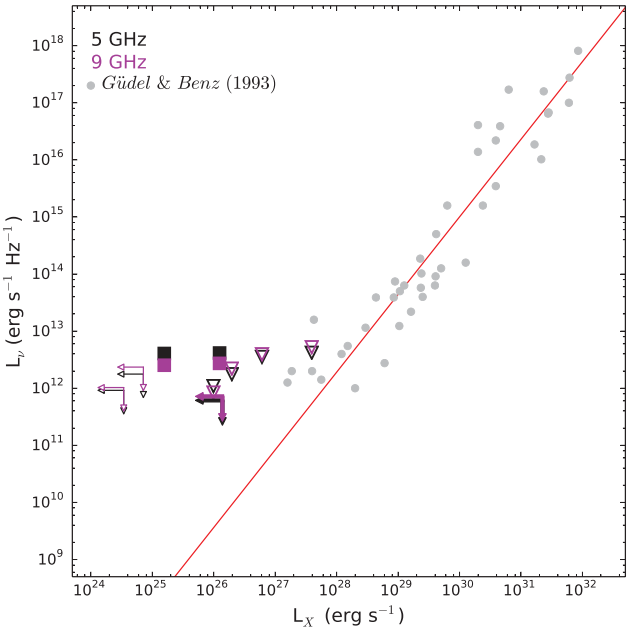

Figure 7. Quiescent radio luminosity as a function of X-ray luminosity for a wide range of coronally active stars. The grey points are the results from Güdel & Benz (1993) and the red-line is a fit to these data from Berger et al. (2010). The results from this survey are given by the black (5 GHz) and magenta (9 GHz) data points. The solid arrows represent the upper limits from stacking the observations with non-detections.

Most of our measured radio upper limits are within 1.5 dex of the GB relation. Given these upper limits the actual radio luminosity of these sources has the potential to be consistent with the GB relation. However for two of our objects, 2MASS J1507476−162738 and 2MASS J02550357−4700509, their measured radio upper limits place them ∼2.6 dex away from the GB relation. This indicates that the measured radio luminosities for these two sources would have to be significantly less than the upper limits in order for them to be consistent with the GB relation.

Following the method outlined in Hancock, Gaensler & Murphy (2011), we stacked 11 of the 12 observations with non-detections. We excluded the observation of 2MASS J00244419−2708242 because we were unable to fully remove a bright field source located at RA = 00:24:36.077 Dec. = −27:07:44.64. In the stacked image we do not detect any radio emission and measure upper limits of 12 μJy (5.5 GHz) and 14.1 μJy (9.0 GHz). Noting that the X-ray luminosities for these sources are $L_x/L_{\rm bol} > -5$ and calculating the effective distance for the staked image to be 6.5 pc, we plot this upper limit in Fig. 7 (solid arrows). Similar to the other upper limits from this survey, this upper limit is 1.3 dex from the GB relation.

6 SUMMARY

From a sample of 15 late-M and L dwarfs, located within 10 pc of the Sun, we have detected quiescent radio emission at frequencies between 4.7 and 9.7 GHz for three sources, 2MASS J1048−3956, 2MASS J0339−3525, and 2MASS J0004−4044. While both 2MASS J1048−3956 and 2MASS J0339−3525 have previous radio detections in the literature, this is the first detection of radio emission from 2MASS J0004−4044. Additionally, we place the first upper limits on the radio emission from 2MASS J0024−2708, 2MASS J03341218−4953322, 2MASS J0340−6724, and 2MASS J02550357−4700509. This increases the number of ultracool

dwarfs studied at radio frequencies to 216, with 17 sources with observed radio emission.

We find that the observed Stokes I and V radio emission from 2MASS J1048−3956, 2MASS J0339−3525, and 2MASS J0004−4044 is well modelled by optically thin gyrosynchrotron emission from a homogenous population of power-law electrons, with density between 10^4 and 10^8 cm^{-3}, spiralling in a magnetic field with a strength of 10–300 Gauss and orientation between 40° and 80°. These parameter ranges are still very large and could benefit from an observation of the spectral turn-over frequency. In the case of gyrosynchrotron emission this frequency is dependent on the electron density and magnetic field orientation and strength (Dulk 1985). Here we assume that this frequency is <4 GHz based on the observed SEDs, however an actual measurement will place stronger constraints on the model parameters.

We also compare the general emission trends of our sample of 15 sources to the results of previous surveys of ultracool dwarfs. As observed in previous radio studies of ultracool dwarfs, we find the observed radio luminosities to be constant with both spectral type and rotation rate. We also find that the ratio of radio to bolometric luminosity to increase towards later type objects and higher rotational velocities. Additionally, using X-ray luminosities from the literature we find that the ratio of radio to X-ray luminosity for 2MASS J1048−3956 and 2MASS J0339−3525 vary significantly from the GB relation. The majority of the radio upper limits are $\lesssim$1.5 dex from the GB relation, however for two source the upper limits differ from GB relation by more than 2 dex. For these two sources the measured radio luminosity would have to be much lower than these upper limits to be consistent with the GB relation.

ACKNOWLEDGEMENTS

The Australia Telescope Compact Array is part of the Australia Telescope which is funded by the Commonwealth of Australia for operation as a National Facility managed by CSIRO. Parts of this research were conducted by the Australian Research Council Centre of Excellence for All–sky Astrophysics (CAASTRO), through project number CE110001020.

REFERENCES

Allred J. C., Hawley S. L., Abbett W. P., Carlsson M., 2006, ApJ, 644, 484
Antonova A., Hallinan G., Doyle J. G., Yu S., Kuznetsov A., Metodieva Y., Golden A., Cruz K. L., 2013, A&A, 549, A131
Benz A. O., Guedel M., 1994, A&A, 285, 621
Berger E., 2002, ApJ, 572, 503
Berger E., 2006, ApJ, 648, 629
Berger E. et al., 2001, Nature, 410, 338
Berger E. et al., 2008, ApJ, 673, 1080
Berger E. et al., 2009, ApJ, 695, 310
Berger E. et al., 2010, ApJ, 709, 332
Burgasser A. J., Putman M. E., 2005, ApJ, 626, 486
Burgasser A. J., Melis C., Zauderer B. A., Berger E., 2013, ApJ, 762, L3
Burgasser A. J., Melis C., Todd J., Gelino C. R., Hallinan G., Bardalez Gagliuffi D., 2015, AJ, 150, 180
Burrows A., Hubbard W. B., Lunine J. I., Liebert J., 2001, Rev. Mod. Phys., 73, 719
Crossfield I. J. M., 2014, A&A, 566, A130
Cutri R. M. et al., 2003, 2MASS All Sky Catalog of point sources. The IRSA 2MASS All–Sky Point Source Catalog, NASA/IPAC Infrared Science Archive
Deacon N. R., Hambly N. C., Cooke J. A., 2005, A&A, 435, 363
Dulk G. A., 1985, ARA&A, 23, 169
Faherty J. K., Burgasser A. J., Cruz K. L., Shara M. M., Walter F. M., Gelino C. R., 2009, AJ, 137, 1
Gizis J. E., Monet D. G., Reid I. N., Kirkpatrick J. D., Liebert J., Williams R. J., 2000, AJ, 120, 1085
Güdel M., Benz A. O., 1993, ApJ, 405, L63
Guenther E. W., Zapatero Osorio M. R., Mehner A., Martín E. L., 2009, A&A, 498, 281
Hallinan G., Antonova A., Doyle J. G., Bourke S., Brisken W. F., Golden A., 2006, ApJ, 653, 690
Hallinan G. et al., 2007, ApJ, 663, L25
Hallinan G. et al., 2015, Nature, 523, 568
Hancock P. J., Gaensler B. M., Murphy T., 2011, ApJ, 735, L35
Hawley S. L., Gizis J. E., Reid I. N., 1996, AJ, 112, 2799
Kao M. M., Hallinan G., Pineda J. S., Escala I., Burgasser A., Bourke S., Stevenson D., 2015, preprint (arXiv:1511.03661)
Leto G., Pagano I., Linsky J. L., Rodonò M., Umana G., 2000, A&A, 359, 1035
Lomb N. R., 1976, Ap&SS, 39, 447
Lynch C., Mutel R. L., Güdel M., 2015, ApJ, 802, 106
Machado M. E., Avrett E. H., Vernazza J. E., Noyes R. W., 1980, ApJ, 242, 336
McLean M., Berger E., Irwin J., Forbrich J., Reiners A., 2011, ApJ, 741, 27
McLean M., Berger E., Reiners A., 2012, ApJ, 746, 23
McMullin J. P., Waters B., Schiebel D., Young W., Golap K., 2007, in Shaw R. A., Hill F., Bell D. J., eds, ASP Conf. Ser. Vol. 376, Astronomical Data Analysis Software and Systems XVI. Astron. Soc. Pac., San Francisco, p. 127
Mohanty S., Basri G., Shu F., Allard F., Chabrier G., 2002, ApJ, 571, 469
Mutel R. L., Molnar L. A., Waltman E. B., Ghigo F. D., 1998, ApJ, 507, 371
Neuhäuser R. et al., 1999, A&A, 343, 883
Neupert W. M., 1968, ApJ, 153, L59
Osten R. A., Jayawardhana R., 2006, ApJ, 644, L67
Osten R. A., Wolk S. J., 2009, ApJ, 691, 1128
Osten R. A., Hawley S. L., Bastian T. S., Reid I. N., 2006a, ApJ, 637, 518
Osten R. A., Hawley S. L., Allred J., Johns-Krull C. M., Brown A., Harper G. M., 2006b, ApJ, 647, 1349
Phan-Bao N., Osten R. A., Lim J., Martìn E. L., Ho P. T. P., 2007, ApJ, 658, 553
Ravi V., Hallinan G., Hobbs G., Champion D. J., 2011, ApJ, 735, L2
Reid I. N., Cruz K. L., Kirkpatrick J. D., Allen P. R., Mungall F., Liebert J., Lowrance P., Sweet A., 2008, AJ, 136, 1290
Reiners A., Basri G., 2008, ApJ, 684, 1390
Reiners A., Basri G., 2009, ApJ, 705, 1416
Reiners A., Basri G., 2010, ApJ, 710, 924
Richards M. T., Waltman E. B., Ghigo F. D., Richards D. S. P., 2003, ApJS, 147, 337
Robinson P. A., Melrose D., 1984, Aust. J. Phys., 37, 675
Rodríguez-Barrera M. I., Helling C., Stark C. R., Rice A. M., 2015, MNRAS, 454, 3977
Route M., Wolszczan A., 2013, ApJ, 773, 18
Sault R. J., Teuben P. J., Wright M. C. H., 1995, in Shaw R. A., Payne H. E., Hayes J. J. E., eds, ASP Conf. Ser. Vol. 77, Astronomical Data Analysis Software and Systems IV. Astron. Soc. Pac., San Francisco, p. 433
Scargle J. D., 1982, ApJ, 263, 835
Schmidt S. J., Cruz K. L., Bongiorno B. J., Liebert J., Reid I. N., 2007, AJ, 133, 2258
Schmidt S. J., Hawley S. L., West A. A., Bochanski J. J., Davenport J. R. A., Ge J., Schneider D. P., 2015, AJ, 149, 158
Stelzer B. et al., 2012, A&A, 537, A94
VanderPlas J., Connolly A. J., Ivezic Z., Gray A., 2012, in Kas K., Chawla N. V., Srivastava A. N., eds, Proc. Conf. Intelligent Data Understanding (CIDU). IEEE, p. 47
West A. A. et al., 2004, AJ, 128, 426
Williams P. K. G., Berger E., 2015, ApJ, 808, 189
Williams P. K. G., Cook B. A., Berger E., 2014, ApJ, 785, 9
Wilson W. E. et al., 2011, MNRAS, 416, 832

This paper has been typeset from a TEX/LATEX file prepared by the author.